

Integral Equations for Boundary Layers with Streamwise Vortices

De Oliveira Andrade, Gael; Timmer, Nando; van Oudheusden, Bas

Publication date

2017

Document Version

Final published version

Published in

52nd 3AF International Conference on Applied Aerodynamics

Citation (APA)

De Oliveira Andrade, G., Timmer, N., & van Oudheusden, B. (2017). Integral Equations for Boundary Layers with Streamwise Vortices. In *52nd 3AF International Conference on Applied Aerodynamics: 27 – 29 March 2017, Lyon – France* Article FP59-AERO2017-deoliveira

Important note

To cite this publication, please use the final published version (if applicable). Please check the document version above.

Copyright

Other than for strictly personal use, it is not permitted to download, forward or distribute the text or part of it, without the consent of the author(s) and/or copyright holder(s), unless the work is under an open content license such as Creative Commons.

Takedown policy

Please contact us and provide details if you believe this document breaches copyrights. We will remove access to the work immediately and investigate your claim.

Integral Equations for Boundary Layers with Streamwise Vortices

Gael de Oliveira⁽¹⁾, Nando Timmer⁽²⁾ and Bas van Oudheusden⁽²⁾

⁽¹⁾Delft University of Technology, Kluyverweg 1, 2629HS Delft, The Netherlands g.l.deoliveiraandrade@tudelft.nl

⁽²⁾Delft University of Technology, Kluyverweg 1, 2629HS Delft, The Netherlands

ABSTRACT

We explore integral boundary layer approximations for shear layer flows with vortex generators. The flow field is decomposed to highlight two phenomena: shear over the wall and vortex-driven mixing of the shear layer. The Navier-Stokes Equations are normalized to identify a new adimensional parameter: the vortex strength number (V_g). Usual boundary layer scales are valid when the vortex strength number (V_g) is of order one or smaller. New Boundary Layer Equations comprising the effect of streamwise vortex filaments are obtained and integrated across a periodic vortex cell. The new integral equations share their structure with the original Von Karmann Integral Equations but use different variables. The deduction concludes with an approximate interaction equation for the construction of generalized closures from the classic set of Swafford turbulent closure relations. The new formulation is solved numerically and it is compatible with future integration in the Xfoil or Rfoil viscous-inviscid airfoil analysis codes.

1. INTRODUCTION

Vortex Generators (VGs) are ubiquitous on modern wind turbine blades[21, 43, 38]. Streamwise vortices are used to improve the lift characteristics of thick airfoils in the inboard half of blades[56, 47]. Secondary flow control[4, 30] is generally applied as a corrective measure and its effect ignored during airfoil design[51, 39]. Airfoil design processes fail to reap the full benefits of vortex generators [7, 2] because of the scarcity of models compatible with the requirements of numerical optimization[18, 70].

Wind energy airfoils[56, 70] are generally optimized by combining a minimization algorithm [14, 15] with a shape parametrization [25, 45] and a viscous-inviscid flow solver[10, 60]. Viscous-inviscid codes are often preferred to Reynolds Averaged Navier Stokes (RANS) models because of their modest computational requirements and superior accuracy in the prediction of very high Reynolds transitional flows [5, 55, 36, 31].

A large share of current vortex generator modelling efforts takes place within the framework of finite volume RANS solvers[11, 16, 59]. Explicit meshing of vortex generator vanes is often considered too costly[13, 33], and most studies resort to variants of the BAY model[3, 26]. BAY approaches extend the momentum equations with a source term for the impact of each vane within the generator array[35, 64, 22, 63]. Vanes aren't fully resolved but localized mesh refinement is necessary to preserve vortex filaments and carries significant computational costs [17].

Tornblom and Johansson[58] adopted a statistical interpretation of vortex filaments to relax computational demands. Statistical models[58, 53, 54] represent the mixing effect of streamwise vortices with a modified closure of the Reynolds Turbulent Stress tensor[29]. Mesh refinement is unnecessary because the vortex filament is not explicitly resolved but manifests as an increase in turbulent diffusion.

Kehro[24] pioneered the statistical representation of vortex filaments within the framework of integral boundary layer theory. Vortex generators appeared as source terms in the shear-lag version[10] of Green's entrainment equation [20]. This approach bypasses significant flow physics and its predictive power is therefore limited. Nonetheless, the absence of competition and its simple integration in Xfoil[10] granted Kehro's model some popularity in the airfoil design community.

Smith constructed the only compact deterministic model describing the entire physics of a boundary layer with imbedded vortex generators[50]. His deduction combined classic turbulent boundary layer theory[46] with modern asymptotic analysis[28] to obtain small perturbation equations attacked with Fourier series expansions. Smith's approach bears remarkable formal beauty and physical insight but practical difficulties hindered its popularity. Major concerns include limited handling of vane-type vortex generators and the inability to incorporate results from phenomenological[23, 61, 40] and empirical studies.

2. BOUNDARY LAYER EQUATIONS

The analysis starts from the idea that the flow is driven by two phenomena: shear over the wall and vortex-driven mixing of the shear layer. Both phenomena are governed by the steady incompressible Navier Stokes equations:

$$\begin{cases} (U \cdot \nabla)U = -\frac{1}{\rho}\nabla P + \nu\Delta U \\ \nabla \cdot U = 0 \end{cases} \quad (1)$$

The phenomenological interpretation of the flow translates into a decomposition of the pressure and velocity fields:

$$\begin{aligned} P &= \bar{P} + \tilde{P} \\ U &= \tilde{U} + \tilde{U} \\ V &= \tilde{V} + \tilde{W} \\ W &= \underbrace{\tilde{W}}_{\text{Shear Layer}} + \underbrace{\tilde{W}}_{\text{Vortical Flow}} \end{aligned} \quad (2)$$

Exact relations between shear and vortical flow components are not defined yet, but expression 2 can already be fed into the Navier Stokes equations (1).

$$\begin{cases} ((\tilde{U} + \tilde{U}) \cdot \nabla)(\tilde{U} + \tilde{U}) = \\ = -\frac{1}{\rho}\nabla P + \nu\Delta(\tilde{U} + \tilde{U}) \\ \nabla \cdot (\tilde{U} + \tilde{U}) = 0 \end{cases} \quad (3)$$

Equation 3 has no direct use but provides a solid foundation to identify dominant terms once the scales of each flow component are assessed.

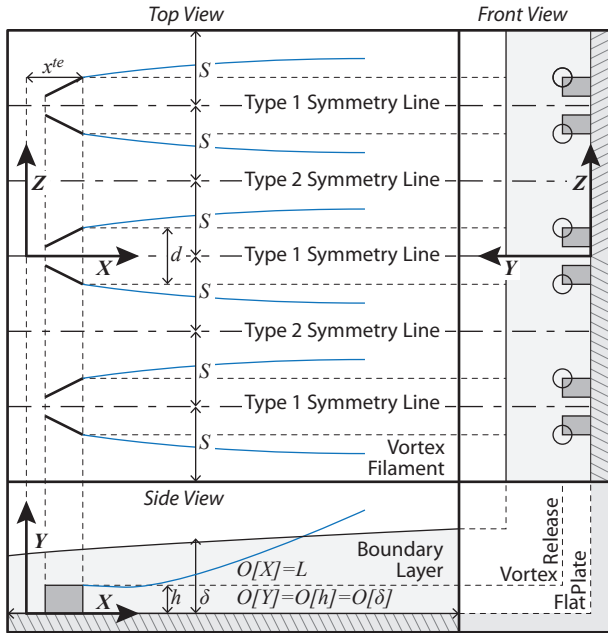


Figure 1: Geometric construction, scales and notation.

Classic boundary layer practice provides reliable order of magnitude estimates for the shear flow components by using figure 3.

$$\begin{aligned} O[X] &= L & O[\tilde{U}] &= U_e \\ O[Y] &= \delta & O[\tilde{V}] &= \frac{\delta U_e}{L} \\ O[\bar{P}] &= \rho U_e^2 & O[\tilde{W}] &= 0 \end{aligned} \quad (4)$$

Streamwise vortices induce normal and spanwise flows (\tilde{V}, \tilde{W}). The order of magnitude of the crossflow vortical components can be estimated from the spatial scales and the expression for the induced field of a planar singular vortex []. The circulation per unit length of streamwise vortices is denoted as Γ and the kinetic energy of the induced flow defines a meaningful gauge for the vortical pressure field.

$$\begin{aligned} O[\bar{P}] &= \frac{\rho}{\delta^2} \left(\frac{\Gamma}{2\pi}\right)^2 & O[\tilde{V}] &= \frac{\Gamma}{2\pi} \frac{1}{\delta} \\ O[Z] &= S & O[\tilde{W}] &= \frac{\Gamma}{2\pi} \frac{1}{\delta} \end{aligned} \quad (5)$$

Vortex filaments exhibit nearly negligible induction in the streamwise direction[61]. The streamwise component \tilde{U} is therefore dominated by the mixing effect of streamwise vortices on the shear layer. \tilde{U} will be referred to as the mixed flow component for the remainder of this communication because it will be assigned the role of an interaction term rather than a “pure” vortical flow component.

A decent but imperfect gauge is obtained by arguing that the mixed flow (\tilde{U}) must be proportional to the normal vortical flow component $O[\tilde{V}]$, the inhomogeneity of the shear field $O[\partial\tilde{U}/\partial Y]$ and the relative length over which mixing occurs $O[X]/O[\tilde{U}]$. One can think of \tilde{U} as a representation of the difference in streamwise momentum between shear flows with and without vortex generators.

$$O[\tilde{U}] \propto \underbrace{\left(\frac{\Gamma}{2\pi} \frac{1}{S}\right)}_{O[\tilde{V}]} \underbrace{\frac{U_e}{\delta}}_{O[\partial\tilde{U}/\partial Y]} \underbrace{\frac{L}{U_e}}_{O[X]/O[\tilde{U}]} = \left(\frac{\Gamma}{2\pi} \frac{1}{S}\right) \left(\frac{L}{\delta}\right) \quad (6)$$

The gauges of expressions 4, 5 and 6 define a linear homeomorphism (7) that maps the flow into adimensional space.

$$\begin{aligned} \bar{u} &= \frac{\tilde{U}}{U_e} & \tilde{u} &= \frac{\tilde{U}}{\left(\frac{\Gamma}{2\pi S}\right)\left(\frac{L}{\delta}\right)} \\ \bar{v} &= \frac{\tilde{V}}{U_e} \left(\frac{L}{\delta}\right) & \tilde{v} &= \frac{\tilde{V}}{\left(\frac{\Gamma}{2\pi} \frac{1}{S}\right)} \\ \bar{w} &= \frac{\tilde{W}}{O[\tilde{W}]} & \tilde{w} &= \frac{\tilde{W}}{\left(\frac{\Gamma}{2\pi} \frac{1}{\delta}\right)} \\ \bar{p} &= \frac{\tilde{P}}{\rho U_e^2} & \tilde{p} &= \frac{\tilde{P}}{\frac{\rho}{\delta^2} \left(\frac{\Gamma}{2\pi}\right)^2} \end{aligned} \quad (7)$$

$$\bar{x} = \frac{X}{L} \quad \bar{y} = \frac{Y}{\delta} \quad \bar{z} = \frac{Z}{S}$$

The homeomorphism defined in expression 7 can be inverted and fed into system 3 to obtain a non-dimensional version of the decomposed Navier Stokes equations from system 3. This step does not require much thinking but involves extremely cumbersome algebraic manipulations

from which we spare readers.

$$\left\{ \begin{aligned}
& (\bar{u} + \lambda \tilde{u}) \left(\frac{\partial \bar{u}}{\partial \bar{x}} + \lambda \frac{\partial \tilde{u}}{\partial \bar{x}} \right) + (\bar{v} + \lambda \tilde{v}) \left(\frac{\partial \bar{u}}{\partial \bar{y}} + \lambda \frac{\partial \tilde{u}}{\partial \bar{y}} \right) + \lambda^2 \tilde{w} \frac{\partial \bar{u}}{\partial \bar{z}} = \\
& = - \left(\frac{\partial \bar{p}}{\partial \bar{x}} + \left(\frac{\delta}{L} \right)^2 \lambda^2 \frac{\partial \bar{p}}{\partial \bar{x}} \right) + \frac{1}{\text{Re}} \left(\frac{\partial^2 \bar{u}}{\partial \bar{x}^2} + \left(\frac{L}{\delta} \right)^2 \frac{\partial^2 \tilde{u}}{\partial \bar{y}^2} \right) + \\
& \quad + \frac{\lambda}{\text{Re}} \left(\frac{\partial^2 \tilde{u}}{\partial \bar{x}^2} + \left(\frac{L}{\delta} \right)^2 \left(\frac{\partial^2 \tilde{u}}{\partial \bar{y}^2} + \left(\frac{\delta}{S} \right)^2 \frac{\partial^2 \tilde{u}}{\partial \bar{z}^2} \right) \right) \\
& (\bar{u} + \lambda \tilde{u}) \left(\frac{\partial \bar{v}}{\partial \bar{x}} + \lambda \frac{\partial \tilde{v}}{\partial \bar{x}} \right) + (\bar{v} + \lambda \tilde{v}) \left(\frac{\partial \bar{v}}{\partial \bar{y}} + \lambda \frac{\partial \tilde{v}}{\partial \bar{y}} \right) + \lambda^2 \tilde{w} \frac{\partial \bar{v}}{\partial \bar{z}} = \\
& = - \left(\frac{L}{\delta} \right)^2 \left(\frac{\partial \bar{p}}{\partial \bar{y}} + \left(\frac{S}{L} \right)^2 \lambda^2 \frac{\partial \bar{p}}{\partial \bar{y}} \right) + \frac{1}{\text{Re}} \left(\frac{\partial^2 \bar{v}}{\partial \bar{x}^2} + \left(\frac{L}{\delta} \right)^2 \frac{\partial^2 \tilde{v}}{\partial \bar{y}^2} \right) + \\
& \quad + \frac{\lambda}{\text{Re}} \left(\frac{\partial^2 \tilde{v}}{\partial \bar{x}^2} + \left(\frac{L}{\delta} \right)^2 \frac{\partial^2 \tilde{v}}{\partial \bar{y}^2} + \left(\frac{\delta}{S} \right)^2 \left(\frac{L}{\delta} \right)^2 \frac{\partial^2 \tilde{v}}{\partial \bar{z}^2} \right) \\
& \left((\bar{u} + \lambda \tilde{u}) \left(\lambda \frac{\partial \tilde{w}}{\partial \bar{x}} \right) + (\bar{v} + \lambda \tilde{v}) \left(\lambda \frac{\partial \tilde{w}}{\partial \bar{y}} \right) + \left(\lambda^2 \tilde{w} \frac{\partial \tilde{w}}{\partial \bar{z}} \right) \right) = \\
& = - \lambda^2 \frac{\partial \bar{p}}{\partial \bar{z}} + \frac{\lambda}{\text{Re}} \left(\frac{\partial^2 \tilde{w}}{\partial \bar{x}^2} + \left(\frac{L}{\delta} \right)^2 \frac{\partial^2 \tilde{w}}{\partial \bar{y}^2} + \left(\frac{L}{\delta} \right)^2 \left(\frac{\delta}{S} \right)^2 \frac{\partial^2 \tilde{w}}{\partial \bar{z}^2} \right) \\
& \left(\frac{\partial \bar{u}}{\partial \bar{x}} + \frac{\partial \bar{v}}{\partial \bar{y}} \right) + \lambda \left(\frac{\partial \tilde{u}}{\partial \bar{x}} + \frac{\partial \tilde{v}}{\partial \bar{y}} + \frac{\partial \tilde{w}}{\partial \bar{z}} \right) = 0
\end{aligned} \right. \quad (8)$$

System 8 highlights the role of two adimensional groups, the Reynolds number (Re) and new parameter denoted as λ . The λ group forms a non-dimensional quantity that characterizes the relative strenght of the vortical flow compared to the shear flow. To the best of our knowledge, this adimensional group (λ) has not been identified before and we propose to call it the Vortex Strenght Number (Vg).

$$\text{Vg} = \lambda = \frac{1}{U_e} \left(\frac{\Gamma}{2\pi S} \right) \left(\frac{L}{\delta} \right) \quad (9)$$

Order of magnitude analysis of the x-momentum equation of system (8) shows that boundary layer thickness depends both on Reynolds number and Vortex Strenght number.

$$O[\delta] = \frac{L}{\sqrt{O[1+\lambda]\text{Re}}}$$

Fig. 2 shows a cloud of points illustrating typical (λ, Re_h) combinations found in the Wendt [65, 66] datasets of vortex generator flows.

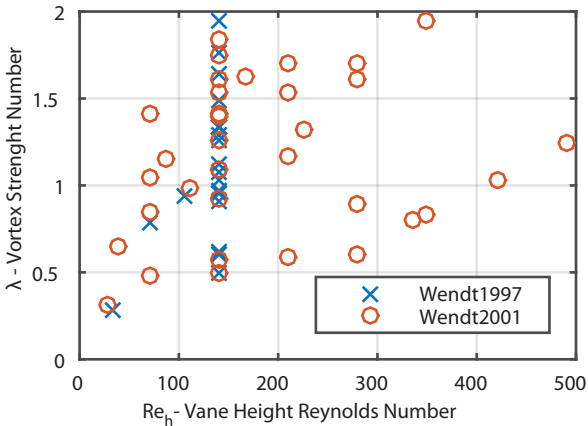


Figure 2: Typical Vortex Strenght Number values.

Vortex strenght number values are generally small, of order one or less. In this range, streamwise vortices affect boundary layer development to a significant extent but have negligible influence from an order of magnitude perspective. Traditional boundary layer scales remain valid.

$$O[\lambda] \leq 1 \quad \Rightarrow \quad \delta = O[\delta] = \frac{L}{\sqrt{\text{Re}}} \quad (10)$$

Expression 10 refines the homeomorphism defined in expression 7 and leads to a compact form of system 8. This form of system?? is normalized and therefore appropriate for estimating the limit as $\text{Re} \rightarrow \infty$. The Prantl[prandtt, kervorkian] limit leads to system 11: a new set of boundary layer equations comprising the effect of streamwise vortices with vortex strenght number λ of order 1 or smaller.

$$\left\{ \begin{aligned}
& (\bar{u} + \lambda \tilde{u}) \left(\frac{\partial \bar{u}}{\partial \bar{x}} + \lambda \frac{\partial \tilde{u}}{\partial \bar{x}} \right) + (\bar{v} + \lambda \tilde{v}) \left(\frac{\partial \bar{u}}{\partial \bar{y}} + \lambda \frac{\partial \tilde{u}}{\partial \bar{y}} \right) + \\
& + \lambda^2 \tilde{w} \frac{\partial \bar{u}}{\partial \bar{z}} = - \frac{\partial \bar{p}}{\partial \bar{x}} + \left(\frac{\partial^2 \bar{u}}{\partial \bar{y}^2} + \lambda \left(\frac{\partial^2 \tilde{u}}{\partial \bar{y}^2} + \left(\frac{\delta}{S} \right)^2 \frac{\partial^2 \tilde{u}}{\partial \bar{z}^2} \right) \right) \\
& 0 = \frac{\partial \bar{p}}{\partial \bar{y}} \\
& (\bar{u} + \lambda \tilde{u}) \left(\lambda \frac{\partial \tilde{w}}{\partial \bar{x}} \right) + (\bar{v} + \lambda \tilde{v}) \left(\lambda \frac{\partial \tilde{w}}{\partial \bar{y}} \right) + \\
& + \left(\lambda^2 \tilde{w} \frac{\partial \tilde{w}}{\partial \bar{z}} \right) = - \lambda^2 \frac{\partial \bar{p}}{\partial \bar{z}} + \lambda \frac{\partial^2 \tilde{w}}{\partial \bar{y}^2} + \lambda \left(\frac{\delta}{S} \right)^2 \frac{\partial^2 \tilde{w}}{\partial \bar{z}^2} \\
& \left(\frac{\partial \bar{u}}{\partial \bar{x}} + \frac{\partial \bar{v}}{\partial \bar{y}} \right) + \lambda \left(\frac{\partial \tilde{u}}{\partial \bar{x}} + \frac{\partial \tilde{v}}{\partial \bar{y}} + \frac{\partial \tilde{w}}{\partial \bar{z}} \right) = 0
\end{aligned} \right. \quad (11)$$

System 11 is subject to a mixed set of boundary conditions. No-slip at the wall and outer velocity matching[28] lead to Neumann conditions summarized in expression 12.

$$\begin{aligned}
\bar{U}|_{Y=0} &= 0 & \bar{U}|_{Y \rightarrow \infty} &= U_e \\
\bar{V}|_{Y=0} &= 0 & & \\
\bar{U}|_{Y=0} &= 0 & \bar{U}|_{Y \rightarrow \infty} &= 0
\end{aligned}, \quad (12)$$

Spanwise flow periodicity manifests in terms of Neumann and Dirichlet constraints expressed with an arbitrary integer $n \in \mathbb{Z}$ in statement 13.

$$\begin{aligned}
\bar{W}|_{Z=nS} &= 0 \\
\bar{U}|_{Z=nS} &= \bar{U}|_{Z=(n+2)S} \\
\frac{\partial \bar{U}}{\partial Z}|_{Z=0} &= \frac{\partial \bar{U}}{\partial Z}|_{Z=-nS}
\end{aligned} \quad (13)$$

System 11 can be integrated across the periodic vortex system, $Y \in [0, \infty]$ and $Z \in [-S, S]$, to obtain a new set of integral equations (14).

$$\left\{ \begin{aligned}
\frac{\partial \hat{\theta}}{\partial X} &= \frac{C_f}{2} - \left(\hat{H}_{12} + 2 \right) \frac{\hat{\theta}}{U_e} \frac{\partial U_e}{\partial x} \\
\frac{\partial \hat{H}_{32}}{\partial X} &= \frac{2C_p}{\theta} - \frac{\hat{H}_{32}}{\theta} \frac{C_f}{2} + \left(\hat{H}_{12} - 1 \right) \frac{\hat{H}_{32}}{U_e} \frac{\partial U_e}{\partial x}
\end{aligned} \right. \quad (14)$$

System 14 shares its structure with the original Von Karman equations (19) but uses different variables defined in expressions 15, 16 and 17. Expression 15 defines average thicknesses:

$$\begin{aligned}
\hat{\delta}_1 &= \frac{1}{S} \int_{-S}^S \int_0^\infty \left(1 - \frac{U}{U_e} \right) dY dZ \\
\hat{\theta} &= \frac{1}{S} \int_{-S}^S \int_0^\infty \left(\frac{U}{U_e} \left(1 - \frac{U}{U_e} \right) \right) dY dZ \\
\hat{\delta}_3 &= \frac{1}{S} \int_{-S}^S \int_0^\infty \left(\frac{U}{U_e} \right) \left(1 - \left(\frac{U}{U_e} \right)^2 \right) dY dZ
\end{aligned} \quad (15)$$

Expression 16 defines generalized shape factors:

$$\begin{aligned}\widehat{H}_{12} &= \widehat{\delta}_1 / \widehat{\theta} \\ \widehat{H}_{32} &= \widehat{\delta}_3 / \widehat{\theta}\end{aligned}\quad (16)$$

And expression 17 defines expectable skin-friction and dissipation coefficients:

$$\begin{aligned}C_{\bar{f}} &= \frac{1}{\frac{1}{2}\rho\bar{U}_e^2 S} \int_{-S}^S \left(\mu \frac{\partial U}{\partial Y} \right) \Big|_{Y=0} dZ \\ \widehat{C}_D &= \frac{\mu}{\rho\bar{U}_e^3 S} \int_{-S}^S \int_0^\infty \left(\frac{\partial U}{\partial Y} \right)^2 + \left(\frac{\partial U}{\partial Z} \right)^2 dY dZ\end{aligned}\quad (17)$$

New integral variables call for the establishment of new closure relations. Section 3 describes a possible strategy to derive new closures from previous practice. Particular emphasis is placed on finding a way to re-use the Swafford and Schlichting closure sets employed in the boundary layer formulation of the Xfoil and Rfoil viscous-inviscid solvers.

3. CLOSURE OF BOUNDARY LAYER EQUATIONS

The systems of decomposed equations presented in section 2 are not closed. The solution of system 11 would require that a clear definition of the shear flow (\bar{U}, \bar{V}) and vortical flow (\tilde{V}, \tilde{W}) components be provided, together with an equation for the evolution of the mixed flow \tilde{U} . Similarly, the solution of system 14 with an integral boundary layer solver would require the provision of new closure relations that are not yet available.

This section takes important steps towards the obtention of a closed set of approximate equations describing the evolution of boundary layers with streamwise vortices. The first steps consist in freezing the definition of pure shear (\bar{U}, \bar{V}) and vortical (\tilde{U}, \tilde{V}) flow components. The deduction proceeds and the main result is an approximate equation for the evolution of mixed flow \tilde{U} . The complete formulation will be closed in section 4.

3.1 Definition of Shear Flow Component

We draw our inspiration from asymptotic analysis[28] and choose to define the shear flow component as if it were locally governed by the classic boundary layer equations which correspond to system 11 when λ tends to 0:

$$\begin{cases} \bar{u} \frac{\partial \bar{u}}{\partial \bar{x}} + \bar{v} \frac{\partial \bar{u}}{\partial \bar{y}} = -\frac{\partial \bar{p}}{\partial \bar{x}} + \frac{\partial^2 \bar{u}}{\partial \bar{y}^2} \\ \frac{\partial \bar{p}}{\partial \bar{y}} = 0 \\ \frac{\partial \bar{u}}{\partial \bar{x}} + \frac{\partial \bar{v}}{\partial \bar{y}} = 0 \end{cases}\quad (18)$$

System 14 can be integrated from the wall to infinity in Y to obtain the classical Von Karman equations (19):

$$\begin{cases} \frac{\partial \theta}{\partial X} = \frac{C_f}{2} - (H_{12} + 2) \frac{\theta}{U_e} \frac{\partial U_e}{\partial x} \\ \frac{\partial H_{32}}{\partial X} = \frac{2C_D}{\theta} - \frac{H_{32}}{\theta} \frac{C_f}{2} + (H_{12} - 1) \frac{H_{32}}{U_e} \frac{\partial U_e}{\partial x} \end{cases}\quad (19)$$

System 19 refers to the usual variables found in classical boundary layer literature [46]:

$$\begin{aligned}\delta_1 &= \int_0^\infty \left(1 - \frac{\bar{U}}{U_e} \right) dY \\ \theta &= \int_0^\infty \left(\frac{\bar{U}}{U_e} \left(1 - \frac{\bar{U}}{U_e} \right) \right) dY \\ \delta_3 &= \int_0^\infty \left(\frac{\bar{U}}{U_e} \right) \left(1 - \left(\frac{\bar{U}}{U_e} \right)^2 \right) dY \\ H_{12} &= \delta_1 / \theta \quad H_{32} = \delta_3 / \theta\end{aligned}\quad (20)$$

The variables defined in expression 20 enable the reconstruction of the shear flow field \bar{U} from either Schlichting[46] or Swafford profiles.

3.2 Definition of Vortical Flow Component

The pure vortical flow components (\tilde{V}, \tilde{W}) are defined as if they were entirely caused by vortex filaments. A strategy for determining the induction of streamwise vortices from a compact set of vortex descriptors will be outlined in section 4. For now, it is sufficient to keep in mind that a simple way to reconstruct the vortical flow field is available.

3.3 Mixed Flow Interaction Equation

We will now focus on the deduction of an approximate equation for the evolution of the mixed flow field \tilde{U} . The first step consists in subtracting the first (X-momentum) equation of system 18 to the corresponding equation of system 11 and rewrite the result into dimensional form.

$$\begin{aligned}(\bar{U} + \tilde{U}) \frac{\partial \tilde{U}}{\partial X} + \left(\tilde{U} \frac{\partial \tilde{U}}{\partial X} + \bar{v} \frac{\partial \tilde{U}}{\partial Y} + \tilde{V} \frac{\partial \tilde{U}}{\partial Y} \right) \\ + \left(\tilde{V} \frac{\partial \tilde{U}}{\partial Y} + \tilde{W} \frac{\partial \tilde{U}}{\partial Z} \right) = \nu \left(\frac{\partial^2 \tilde{U}}{\partial Y^2} + \frac{\partial^2 \tilde{U}}{\partial Z^2} \right)\end{aligned}\quad (21)$$

In the absence of strong pressure gradients, the streamwise component of the shear flow changes very slowly in the longitudinal direction. The normal component of the shear flow is then equally small, given that \bar{V} and $\partial \bar{U} / \partial X$ are coupled by the continuity equation through the wall impermeability condition. It is therefore expectable that two convective terms from equation 21 will be negligibly small in flows with mild pressure gradients.

$$\begin{aligned}O \left[\tilde{U} \frac{\partial \tilde{U}}{\partial X} \right] \approx O \left[\tilde{V} \frac{\partial \tilde{U}}{\partial Y} \right] \} \Rightarrow \tilde{U} \frac{\partial \tilde{U}}{\partial X} \ll \tilde{V} \frac{\partial \tilde{U}}{\partial Y} \\ \bar{V} \ll \tilde{V} \} \\ O \left[\bar{V} \frac{\partial \tilde{U}}{\partial Y} \right] \approx O \left[\tilde{V} \frac{\partial \tilde{U}}{\partial Y} \right] \} \Rightarrow \bar{V} \frac{\partial \tilde{U}}{\partial Y} \ll \tilde{V} \frac{\partial \tilde{U}}{\partial Y}\end{aligned}\quad (22)$$

The expectations of expression 22 suggest that equation 23 represents a reasonable approximation of equation 21.

$$\begin{aligned}(\bar{U} + \tilde{U}) \frac{\partial \tilde{U}}{\partial X} + \left(\tilde{V} \frac{\partial \tilde{U}}{\partial Y} \right) \\ + \left(\tilde{V} \frac{\partial \tilde{U}}{\partial Y} + \tilde{W} \frac{\partial \tilde{U}}{\partial Z} \right) = \nu \left(\frac{\partial^2 \tilde{U}}{\partial Y^2} + \frac{\partial^2 \tilde{U}}{\partial Z^2} \right)\end{aligned}\quad (23)$$

Equation 23 is best interpreted with custom differential operators: a lagrangian derivative for the streamwise (X)

direction, and a nabla symbol for the normal-spanwise ($Y - Z$) plane.

$$\begin{aligned} \nabla^{yz} &= \left(\frac{\partial}{\partial Y}, \frac{\partial}{\partial Z} \right) \\ \frac{D}{DT_x} &= \frac{\partial}{\partial T} + U \frac{\partial}{\partial X} = (\tilde{U} + \tilde{U}) \frac{\partial}{\partial X} \end{aligned} \quad (24)$$

The operators defined in expression 24 help rewrite equation 23 in a simple form that highlights its qualitatively parabolic nature in the longitudinal direction:

$$\frac{D\tilde{U}}{DT_x} + \underbrace{((\tilde{V}, \tilde{W}) \cdot \nabla^{yz})}_{\text{advection}} \tilde{U} = \underbrace{\nu \nabla_{yz}^2 \tilde{U}}_{\text{diffusion}} - \underbrace{\tilde{v} \frac{\partial \tilde{U}}{\partial Y}}_{\text{source}} \quad (25)$$

Equation 25 displays the typical structure of a 2d advection-diffusion equation with source terms. Advection and diffusion take place in the YZ plane, while the X coordinate indirectly plays the role of time.

The mixed flow field \tilde{U} departs from initially homogeneous conditions ($\tilde{U} = 0$ at $X = X_0$) and receives momentum through a source term that is proportional to the normal vortical component \tilde{V} and the inhomogeneity $\partial \tilde{U} / \partial Y$ of the shear flow \tilde{U} . As soon as it is seeded, the mixed flow field \tilde{U} evolves along the X/T_x dimension under the effect of diffusion and advection by vortical flow components (\tilde{V}, \tilde{W}).

Equation 25 treats the mixed flow field as if it were a passive scalar transported by vortex induced velocities and diffused only in the crossflow plane. The \tilde{U} field is also advected in the X direction by the streamwise component of the shear flow and convected by itself in that same direction. Convective and advective processes along the X dimension are included in equation 25 but hidden by the unusual differential operators of expression 24.

3.4 Connection between flow Fields

The mixed flow field \tilde{U} connects the flow field of a pure shear layer \tilde{U} with the total flow field U of a boundary layer with streamwise vortices. Integral quantities for the total flow field (defined in expressions 15-17) are computed by combining the mixed flow field with a reconstruction of the pure shear flow field from its integral quantities (defined in expressions ...-...).

Knowledge about the mixed flow field \tilde{U} is obtained by solving equation 25. The solution of equation 25 is described in section 5 but the procedure requires detailed knowledge about vortical flow components (\tilde{V}, \tilde{W}). The next section therefore outlines a strategy for modelling the evolution of vortex filaments computing vortical flow components (\tilde{V}, \tilde{W}) to close equations (25) and (19 or 14).

4. EVOLUTION OF VORTEX DESCRIPTORS

Vortical flow components can be reconstructed from a small set of parameters describing the local state and position of vortex filaments. Westphal[69] called these parameters vortex descriptors. This section describes a

collection of phenomenological models that can be combined to compute the evolution of vortex descriptors: circulation per unit length Γ , peak vorticity ω^{max} and core center (Y^v, Z^v).

4.1 Initial Circulation, Peak Vorticity and Induced Field

The generation of vorticity at the vane tip has been studied extensively since Taylor's first demonstration of the effectiveness of vortex generators. Early studies considered each vane as a small uncambered wing with finite aspect ratio. According to this philosophy, the circulation of each vortex filament was estimated from Prandtl's lifting line solution for a finite flat plate wing:

$$\Gamma_v = \frac{\pi \alpha_v c_v U_e}{1 + \frac{2}{AR}}$$

This approach neglected low aspect ratio effects and ignored the immersion of the vane in the boundary layer. Wendt circumvented these limitations with a data-driven expression for the initial circulation of streamwise vortices[65, 66, 68]. Expression 26 uses four constants (k_1 to k_4) to incorporate empirical results from extensive parametric studies[66] conducted at the Langley internal flow facility[42].

$$\Gamma_v = \left(\frac{k_1 \alpha_v c_v U_e}{1 + \frac{k_2}{AR}} \right) \tanh \left(k_3 \left(\frac{h}{\delta} \right)^{k_4} \right) \quad (26)$$

Prediction of filament strength is relatively straightforward because it depends on a process governed primarily by inciscid phenomena. But real fluids are viscous and filament vorticity spreads over a diffusing core due to shear stresses and turbulent transport. The phenomenon is overly complex but its interpretation is simplified by noticing that the core of a Lamb vortex[44, 57] is defined by the maximum value of local vorticity[69].

Wendt[65, 66] deployed angular momentum conservation arguments to estimate peak vorticity ω^{max} at the trailing edge of vortex generator vanes. The resulting expression (27) uses a single empirical constant ($\xi = 0.29$) tuned from the same dataset as expression 26 .

$$\omega^{max} = \frac{\Gamma_v^3 (\beta - 1)^2}{2\pi^3 (\alpha_v h_v c_v U_e)^2} \quad , \quad \beta = \frac{1}{2\xi^2 \left(1 - e^{-\frac{1}{2}} \right)^2} \quad (27)$$

Expressions ... and ... plea for representing the induction of the vortex filament with a Lamb vortex. Expression 28 describes the magnitude of the induced velocity field of a Lamb vortex contained in the $y - z$ plane. It is used to compute vortical flow components (\tilde{V}, \tilde{W}) in section 5.

$$|\tilde{V} + \tilde{W}| = \frac{\Gamma}{2\pi r} \left(1 - e^{\left(-\frac{\pi \omega^{max}}{\Gamma} r^2 \right)} \right) \quad (28)$$

Expression 28 is written in the form proposed by Wendt[65] and provides a reasonable estimation for the cross-wise induction of streamwise vortices with negligible curvature. More sophisticated models could be proposed by resorting to the work of Velte and Gamiz[61, 12].

4.2 Advection of Streamwise Vortices

Vortex generator vanes behave like small wings and release vorticity at the tip. Trailing vorticity is transported and lumps into filaments. These filaments are initially aligned with the streamwise direction but acquire some curvature as they deform under their mutual induction and wall influence. This phenomenon was first modelled by Jones [23] using inviscid induction functions and the method of images on a periodic vortex system. Jones

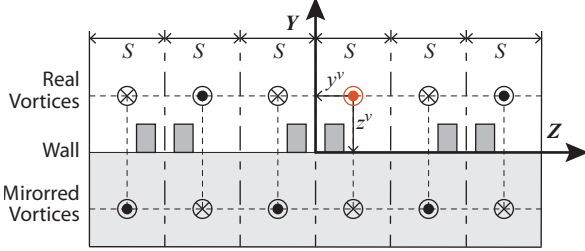


Figure 3: Jones (1957) replicated vortex system including method of images.

solved his model analytically but Wendt[67] suggested to recast his approach into a system of ODEs, as in expression 29.

$$\begin{cases} \frac{dY^v}{dX} = \frac{\tilde{V}_v}{U_v} \\ \frac{dZ^v}{dX} = \frac{\tilde{W}_v}{U_v} \end{cases} \quad \begin{aligned} U_v &= (\bar{U} + \tilde{U})|_{(X, Y^v, Z^v)} \\ \tilde{V}_v &= (\tilde{V})|_{(X, Y^v, Z^v)} \\ \tilde{W}_v &= (\tilde{W})|_{(X, Y^v, Z^v)} \end{aligned} \quad (29)$$

Vortical velocities \tilde{V} and \tilde{W} are computed with a numerically replicated version of the Lamb induction function (28) in accordance with the recommendations of Logdberg[32]. Variables Y^v and Z^v denote the center of the reference vortex core at a given streamwise position X , and vortex core positions are initialized at the trailing edge of the vane tip.

$$\begin{cases} Y_0^v = h^{vg} \\ Z_0^v = d^{vg}/2 \end{cases}$$

Jones' approach assumes that curvature is small to model local induction with infinite lines of vorticity that intersect the crossflow plane at the local core height $Y_{(X^v)}^v$ and spanwise $Z_{(X^v)}^v$ position. This approximation is consistent with the results of asymptotic analysis [57] and justifies the use of planar induction functions. It is known to yields accurate predictions for the initial development of vortex filaments [41, 32].

4.3 Transverse Diffusion of Streamwise Vortices

Vorticity diffuses mostly in the crossflow plane as the filament gets convected downstream. This section describes a simple model for the diffusion of vortex cores similar to the ones proposed by Squire[52] and Wendt [67]. All three approaches build upon the Lamb solution for the

time evolution of the velocity field of a diffusing planar vortex.

$$|\tilde{V} + \tilde{W}| = \frac{\Gamma}{2\pi r} \left(1 - e^{(-\frac{1}{4vt^v} r^2)}\right) \quad (30)$$

The induced velocity field of the Lamb vortex can also be represented in terms of current circulation and peak vorticity using expression 28. Matching equation 30 with equation 28 provides a crude relation between the "age" of the vortex core t^v and the rate at which peak vorticity $\omega_{(t^v)}^{max}$ decreases.

$$\frac{\pi}{\Gamma} \omega_{(t^v)}^{max} = \frac{1}{4vt^v} \Rightarrow \frac{d\omega_{(t^v)}^{max}}{dt^v} = -\frac{\Gamma}{4\pi v} \left(\frac{1}{t^v}\right)^2 \quad (31)$$

Vortex filaments form over the entire chord of the vane tip, so there is no unambiguous definition of the filament origin or "age"[40]. Even so, the initial peak vorticity ω_0^{max} can be fed into expression 31 to obtain a crude estimate of the virtual "age" of the vortex core at the trailing edge of the vane tip:

$$t_0^v = \frac{\Gamma}{4\pi v \omega_0^{max}}$$

The differential of the streamwise position (dX_v) of the vortex core center can be related with the differential of its age (dt_v) through the streamwise convection velocity U_v :

$$dt^v = \frac{1}{U_v} dX_v \Leftrightarrow U_v = \frac{dX_v}{dt^v} \quad (32)$$

The combination of equations 31 and 32 yields a system of ordinary differential equations that describe the diffusion of vortex filament cores by dampening peak vorticity.

$$\begin{cases} \frac{d\omega_{(t_0^v)}^{max}}{dt^v} = -\frac{\Gamma}{4\pi v} \left(\frac{1}{t^v}\right)^2 \\ \frac{dt^v}{dX} = \frac{1}{U_v} \end{cases} \quad \text{with} \quad \begin{aligned} \omega_{(t_0^v)}^{max} &= \omega_0^{max} \\ t_0^v &= \frac{\Gamma}{4\pi v \omega_0^{max}} \\ X_0 &= x^{TE} \end{aligned} \quad (33)$$

System 33 is subject to Dirichlet initial boundary conditions and its integration with the Integral Boundary Layer Equations is straightforward.

5. INTEGRATION OF THE INTERACTION EQUATION

The mixed flow \tilde{U} interaction equation (25) is a partial differential equation of qualitatively hyperbolic nature. Equation 25 is semi-discretized into a set of qualitatively parabolic ordinary differential equations[27, 26] so that it can be integrated together with the Integral Boundary Layer (14 or 19) and vortex descriptor equations (29 and 33).

Equation 34 achieves a finite-difference semi-discretization of equation (25) over a plaided collection of points (Y_{ij}, Z_{ij}) in the crossflow plane $i, j \in [1, N] \in \mathbb{N}$. Vortical components $(\tilde{V}_{ij}, \tilde{W}_{ij})$ are computed over the mesh from vortex descriptors $(\Gamma, \omega^{max}, Y^v, Z^v)$ using expression 28 while the shear flow \tilde{U}_{ij} is reconstructed

from integral quantities (20).

$$\begin{aligned} \frac{D\tilde{U}_{ij}}{DT_x} + \left((\tilde{V}_{ij}, \tilde{W}_{ij}) \cdot \nabla_{ij}^{yz} \right) \tilde{U}_{ij} &= \\ &= \nu \Delta_{ij}^{yz} \tilde{U}_{ij} - \left((\tilde{V}_{ij}, \tilde{W}_{ij}) \cdot \nabla_{ij}^{yz} \right) \tilde{U}_{ij} \quad (34) \\ \tilde{V}_{ij} &= \tilde{V}_{(X,Y_{ij},Z_{ij})} \quad \tilde{W}_{ij} = \tilde{W}_{(X,Y_{ij},Z_{ij})} \end{aligned}$$

The ∇_{ij}^{yz} symbol denotes a discrete first-order central difference operator and Δ_{ij}^{yz} embodies a discrete Laplacian operator. Both operators include single sided differences on the domain boundaries and are filtered for explicit enforcement of Neumann and Dirichlet boundary conditions. A Lagrangian perspective is adopted for the longitudinal direction, and the X-coordinate is treated as the equivalent of a time. Expression 24 is used to establish a first-order accurate correspondence between steps in time (ΔT_x) and space (ΔX):

$$(\bar{U}_{ij}^n + \tilde{U}_{ij}^n) \Delta T_x = \Delta X \quad (35)$$

Superscript (n) denotes the current step and a first-order explicit Euler scheme is adopted for integrating numerically along the streamwise direction. The semi-discrete equation (34) then transforms into a fully discrete evolution problem (36) subject to initial boundary conditions.

$$\begin{cases} \tilde{U}_{ij}^{n+1} = \tilde{U}_{ij}^n + \frac{D\tilde{U}_{ij}^n}{DT_x} \Delta T_x \\ \frac{D\tilde{U}_{ij}^n}{DT_x} = \nu \Delta_{ij}^{yz} \tilde{U}_{ij}^n - \left((\tilde{V}_{ij}^n, \tilde{W}_{ij}^n) \cdot \nabla_{ij}^{yz} \right) \tilde{U}_{ij}^n \\ \quad - \left((\tilde{V}_{ij}^n, \tilde{W}_{ij}^n) \cdot \nabla_{ij}^{yz} \right) \tilde{U}_{ij}^n \end{cases} \quad (36)$$

The equivalent time step ΔT_x is capped to respect a Courant-Friedrichs-Lewy condition[6] based on cross-flow mesh spacing and vortical velocities. Artificial viscosity is added to maintain modest Peclet mesh numbers without incurring into unacceptable computational costs[27].

Artificial diffusion has minimal impact on the final solution because the finite-difference method only deals with the mixed flow field (\tilde{U}). Vortex cores do not dissipate under the effect of numerical viscosity because they evolve with the ODE's of system 29 and 33.

6. RESULTS AND VALIDATION

There is ample literature describing experimental studies involving shear flows with streamwise vortices. Important early experiments were conducted by Schubauer and Spangenberg[47], Westphal[69] and the group of Bradshaw[48, 4, 37]. Hot-wire anemometry is losing favour in recent experimental campaigns[19] as flow measurements increasingly employ Particle Image Velocimetry (PIV) for both airfoil [62, 34] and flat plate[1, 8, 32, 49] configurations.

Baldacchino[1] conducted a recent series of experiments in TU-Delft's Boundary Layer Tunnel (BLT)[9]. Different types of vortex generators were tested on flat plates subjected to null and adverse pressure gradients[1] in straight and yawed inflow. Baldacchino's simplest

Vane Height	h	5mm
Vane Chord	c	12.5mm
T.E. Separation	d	12.5mm
Vane Nominal AOA	α	18°
Simmetry Width	S	15mm
Edge Velocity	U_e	15.16m/s

Table 1: Description of Experimental Conditions[1]

case, rectangular vane type vortex generators in a straight periodic arrangement, provide an ideal sandbox for the validation of the formulation presented throughout this communication.

The reader is referred to reference[1] for a detailed description of the experimental setup, but table 1 describes vane characteristics and external inflow conditions. Flow velocities were captured throughout several crossflow planes over a PIV window of about $47 \times 33mm$ covered by 499x360 data pixels. Initial conditions were determined from a set of verification measurements conducted on the baseflow, that is, in the absence of actuation devices. The BLT tunnel boasts a strong concentration ratio (about 16:1) to minimize turbulence and a long (5.4m) wide test-section ($1.25m \times 0.25m$) to minimize end effects. There is, however, some spanwise irregularity of the unactuated baseflow. Initial conditions are not perfectly defined at the stance where the vane trailing edge is placed when actuating the flow. Fig. 4 shows the spanwise variation of the shape factor and momentum reynolds thickness at the starting point of the numerical procedure.

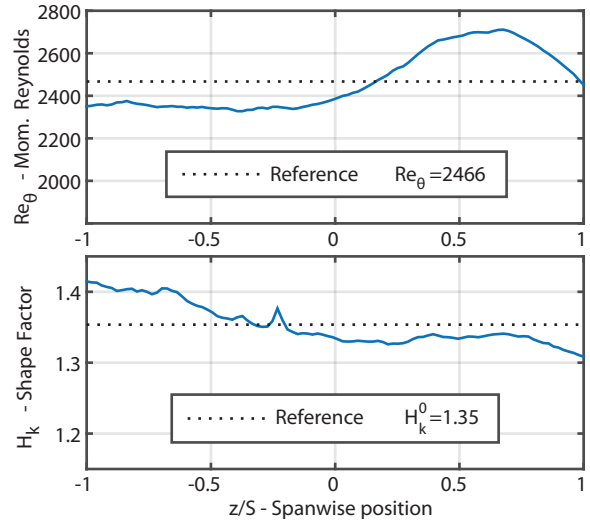


Figure 4: Initial Conditions at Vane Trailing Edge

Average values are taken as reference and the Swafford profile yields a fair reconstruction of the shear velocity field from classical boundary layer descriptors (\bar{H} , $Re_{\bar{\theta}}$). A comparison between the experimental baseflow and the reconstructed baseflow is shown on fig. 5. The semilogarithmic plots highlight the imperfection of turbulent boundary layer theory, even for simple, unactuated flat plate flows[46, 4].

The limitations of classical turbulent boundary layer theory are significant. Integral models can nonethe-

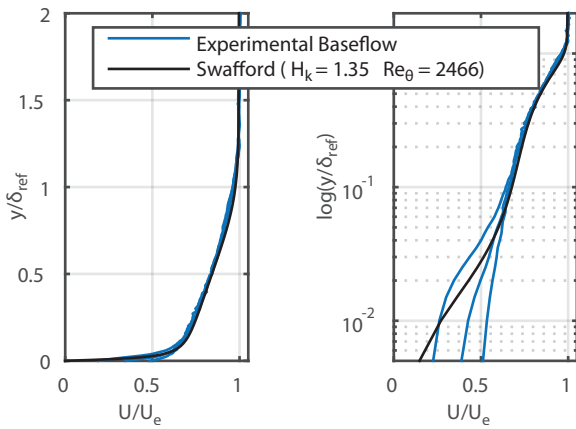


Figure 5: Measured and Reconstructed Velocity Profiles

less produce relevant predictions for both qualitative and quantitative purposes owing to their ability to single out key phenomena and incorporate experimental data. Fig. 6 shows a comparison between measured and predicted velocity profiles for Baldacchino’s simplest vortex generator flow, under the conditions described in tab. 1.

The proposed formulation captures the key physics of vortex generator flows: mixing is accurately represented in the early flow development phase, up to $10h$, and a wide region of accelerated flow forms throughout the entire span as the actuated boundary layer develops further downstream. The phenomenon is the combined product of mixing and movement of vortex core pairs: first towards the wall, then away from each other and finally from the wall. Cores smoothen as they move downstream and so does the mixed flow field.

Results display overall qualitative agreement but quantitative agreement differs throughout flow regions. Fig. 7 sheds some light on the discrepancies by displaying complete velocity fields. The experimental flow field is smoother than the predicted field near the edge of the boundary layer and sharper near the wall (greater effect of actuation on skin-friction). These differences highlight that the present formulation ignores the effect of turbulent mixing on the transport of mixed flow.

The inclusion of a Prandtl mixing length turbulence model in equation 25 would certainly bring significant benefits. Such a model could be driven by the shear-lag version of Green’s equation and its implementation is rather straightforward. The beneficial effect of added diffusion can be witnessed by running the model with coarser grids that required greater artificial viscosity for the stabilization of the finite-difference method.

A detailed investigation of the effect of numerical parameters, including a formal convergence study and public unit test validations of each model will be the object of later research and communications. Such an endeavour will also enable the identification of key calibration parameters to benefit from the greatest advantages of integral boundary layer models: the ability to integrate data from experimental sources and validate submodels separately.

7. CONCLUSION

The present communication explored integral boundary layer approximations for shear layer flows with streamwise vortices like those generated by vortex generators. The flow field was decomposed to highlight the phenomena that dominate near-wall flow: shear over the wall and vortex-driven mixing of the shear layer.

Counter-rotating vortex filaments were considered to exploit flow periodicity, propose meaningful scales and rewrite the Navier-Stokes Equations into decomposed nondimensional variables. The Non-dimensional Navier-Stokes Equations highlight the role of two adimensional parameters: chord Reynolds number (Re) and the newly found vortex strength number (Vg).

Order of magnitude analysis revealed that usual boundary layer scales are still valid when the vortex strength number (Vg) is of order one or smaller. Under this restriction, new Boundary Layer Equations comprising the effect of streamwise vortex filaments were obtained and integrated across a periodic vortex cell system. The new Integral Boundary Layer Equations share their structure with the original Von Karmann Integral Equations but use different variables.

New variables motivated the need for new closure relations and the deduction proceeded with an approximate interaction equation for the construction of generalized closures from the classic set of Swafford turbulent closure relations. The new equations were solved with a direct integral boundary layer solver including additional equations for the evolution of streamwise vortex filaments. Filament strength was estimated with the Wendt model, cores were advected with a differential equation based on Jones ideas and diffused with Squire’s approach.

The entire formulation consists of ordinary differential equations whose structure is compatible with future integration in the Xfoil or Rfoil viscous-inviscid airfoil analysis codes. Future efforts will focus on unit tests to validate each module, implement it in the Rfoil viscous-inviscid solver and ultimately enable the optimization of airfoils for the employment of vortex generators.

REFERENCES

- [1] D. Baldacchino, D. Ragni, C.S. Ferreira, and G.J.W. van Bussel. Towards integral boundary layer modelling of vane-type vortex generators. In *45th AIAA Fluid Dynamics Conference*, volume AIAA 2015-3345, 2015.
- [2] E.C. Battle, R. Pereira, M. Kotsonis, and G. de Oliveira. Airfoil optimisation for dbd plasma actuator in a wind energy environment: Design and experimental study. In *55th AIAA Aerospace Sciences Meeting*, volume AIAA 2017-1578, 2017.
- [3] E.E. Bender, B.H. Anderson, and P.J. Yagle. Vortex generator modelling for navier-stokes codes. In *3rd ASME/JSME Joint Fluids Engineering Conference*, volume FEDSM99-6919, 1999.

- [4] P. Bradshaw. Turbulent secondary flows. *Ann. Rev. Fluid Mechanics*, 19:53–74, 1987.
- [5] O. Ceyhan et al. Summary of the blind test campaign to predict the high reynolds number performance of du00-w-210 airfoil. In *35th Wind Energy Symposium*, volume AIAA 2017-0915, 2017.
- [6] R. Courant, K. Friedrichs, and H. Lewy. On the partial difference equations of mathematical physics. *IBM J. of Res. and Dev.*, 11(2):215–234, 1967.
- [7] G. de Oliveira. Wind turbine airfoils with boundary layer suction, a novel design approach. *Msc Thesis, Delft University of Technology*, 2011.
- [8] G. Di Cicca, G. Iuso, P. Spazzini, and M. Onorato. Piv study of the influence of large-scale streamwise vortices on a turbulent boundary layer. *Experiments in Fluids*, 33(5):663–669, 2002.
- [9] E. Dobbinga. Grondslagen voor het ontwerp van een grenslaagtunnel. Technical report, TH-Delft Vliegtuigbouwkunde 126, 1968.
- [10] M. Drela. Xfoil: An analysis and design system for low reynolds number airfoil. In *Low Reynolds Number Aerodynamics, Springer-Verlag, Lec. Notes in Eng.*, volume 54, 1989.
- [11] J.C. Dudek. Modeling vortex generators in the wind-us code. In *48th AIAA Aerospace Sciences Meeting*, volume AIAA-2010-32, 2010.
- [12] U. Fernandez-Gamiz, C.M. Velte, P.E. Rethore, N.N. Sorensen, and E. Egusquiza. Testing of self-similarity and helical symmetry in vortex generator flow simulations. *Wind Energy*, 19:1043–1052, 2016.
- [13] U. Fernandez-Gamiz, G. Zamorano, and E. Zulueta. Computational study of the vortex path variation with vg heigh. *J. Phys. Conf. Ser.*, 524:012024, 2014.
- [14] R. Fletcher. *Practical methods of optimization*. John Wiley Sons, 1987, 2nd Ed.
- [15] R. Fletcher. *Multi-Objective Optimization using Evolutionary Algorithms*. John Wiley Sons, 2001.
- [16] L. Florentie, A.H. van Zuijlen, and H. Bijl. Towards a multi-fidelity approach for cfd simulations of vortex generator arrays. In *6th European Conference on Computational Fluid Dynamics (ECFD VI)*, volume 1879, 2014.
- [17] L. Florentie, A.H. van Zuijlen, S.J. Hulshoff, and H. Bijl. Effectiveness of side force models for flow simulations downstream of vortex generators. *AIAA Journal*, 2016.
- [18] P. Fuglsang, C. Bak, M. Gaunaa, and I. Antoniou. Design and verification of the riso-b1 airfoil family for wind turbines. *Journal of Solar Energy Engineering*, 126:1002–1010, 2004.
- [19] G. Godard and M. Stanislas. Control of a decelerating boundary layer. part 1: Optimization of passive vortex generators. *Aerospace Science and Technology*, 10(3):181–191, 2006.
- [20] J.E. Green. Application of head’s entrainment method to the prediction of turbulent boundary layers and wakes in compressible flow. Technical report, British ARC RM-3788, 1976.
- [21] D.A. Griffin. Investigation of vortex generator for augmentation of wind turbine power performance. Technical report, NREL/SR-440-21399, 1996.
- [22] A. Jirasek. A vortex generator model and its application to flow control. In *22nd AIAA Applied Aerodynamics Conference*, volume AIAA-2004-4975, 2004.
- [23] J.P. Jones. The calculation of the paths of vortices from a system of vortex generators, and a comparison with experiment. Technical report, British ARC CP-361, 1957.
- [24] M. Kehro and B. Kramer. Enhanced airfoil design incorporating boundary layer mixing devices. *41st AIAA Aerospace Sciences Meeting and Exhibit*, AIAA 2003-0211, 2003.
- [25] B.M. Kulfan and J.E. Bussoletti. Fundamental parametric geometry representations for aircraft component shapes. In *1th AIAA/ISSMO Multidisciplinary Analysis and Optimization Conference*, volume AIAA 2006-6948, 2006.
- [26] W.G. Kunik. Application of a computational model for vortex generators in subsonic internal flows. In *AIAA/ASME/SAE/ASEE 22nd Joint Propulsion Conference*, volume AIAA-86-1458, 1986.
- [27] D. Kuzmin. A guide to numerical methods for transport equations. Technical report, Friedrich-Alexander Universitat, Erlangen-Nuernberg, 2010.
- [28] P.Y. Lagree. *Multiscale Hydrodynamic Phenomena: Matched Asymptotic Expansions*. Course Notes, Paris Jussieu, 2016.
- [29] B.E. Launder, G.J. Reece, and W. Rodi. Progress in the development of a reynolds stress turbulence closure. *J. Fluid Mech.*, 68 (3):537–566, 1975.
- [30] J.C. Lin. Review of research on low-profile vortex generators to control boundary-layer separation. *Progress in Aerospace Sciences*, 38(4-5):389–420, 2002.
- [31] E. Llorente, A. Gorostidi, M. Jacobs, W.A. Timmer, X. Munduate, and O. Pires. Wind tunnel tests of wind turbine airfoils at high reynolds numbers. *J. Phys.: Conf. Ser.*, 524:012012, 2014.
- [32] O. Logdberg, J.H.M. Fransson, and P.H. Alfredsson. Streamwise evolution of longitudinal vortices in a turbulent boundary layer. *Journal of Fluid Mechanics*, 623:27–58, 2009.

- [33] M. Manolesos, N.N. Sorensen, N. Troldborg, G. Papadakis, and S. Voutsinas. Computing the flow past vortex generators: Comparison between rans simulations and experiments. *J. Phys.: Conf. Ser.*, 753:022014, 2016.
- [34] M. Manolesos and S.G. Voutsinas. Experimental investigation of the flow past passive vortex generators on an airfoil experiencing three-dimensional separation. *J. Wind. Eng. Ing. Aerodyn.*, 142:130–148, 2015.
- [35] N.E. May. A new vortex generator model for use in complex configuration cfd solvers. In *19th Applied Aerodynamics Conference*, volume AIAA-2001-2434, 2001.
- [36] B. Mendez, N. Sorensen, N. Ramos, O. Ceyhan, J. Prospathopoulos, and G. Papadakis. 2d airfoil polars for the avatar rotor. Technical report, AVATAR Project Report WP2.1, 2014.
- [37] R.D. Metha and P. Bradshaw. Longitudinal vortices imbedded in turbulent boundary layers. part 1. vortex pair with 'common flow' upwards. *Journal of Fluid Mechanics*, 188:529–546, 1988.
- [38] H. Mueller-Vahl, G. Pechlivanoglou, C.N. Nayeri, and C.O. Paschereit. Vortex generators for wind turbine blades: A combined wind tunnel and wind turbine parametric study. In *ASME Turbo Expo 2012: Turbine Technical Conference and Exposition*, volume 6, 2012.
- [39] Fouatih O.M., M. Medale, O. Imine, and B. Imine. Design optimization of the aerodynamic passive flow control on naca 4415 airfoil using vortex generators. *European Journal of Mechanics - B/Fluids* 56 December 2015, 56:82–96, 2016.
- [40] E.H. Oon. Decay of trailing vortices. Technical report, British ARC CP-1238, 1973.
- [41] H.H. Pearcey. Introduction to shock-induced separation and its prevention by design and boundary layer control. In *Boundary Layer and Flow Control*, volume 2, pages 1167–1344, 1961.
- [42] A.R Porro, W.R. Hingst, C.A. Wasserbauer, and T.B. Andrews. The nasa lewis reseach center internal fluid mechanics facility. Technical report, NASA TM-105187, 1991.
- [43] Siemens Wind Power. Lowering the cost of energy by smart technology. In *Fact Sheet: Rotor Blades*, 2012.
- [44] P.G. Saffman, M.J. Ablowitz, J. Hinch, J.R. Ockendon, and P.J. Olver. *Vortex dynamics*. Cambridge University Press, 1992.
- [45] N.P. Salunke, R.A. Juned Ahamad, and S.A. Channiwala. Airfoil parameterization techniques: A review. *American Journal of Mechanical Engineering*, 2.4:99–102, 2014.
- [46] H. Schlichting. *Boundary Layer Theory*. McGraw-Hill, 1979, 7th Ed.
- [47] G.B. Schubauer and W.G. Spangenberg. Forced mixing in boundary layers. *Journal of Fluid Mechanics*, 8(5):10–32, 1960.
- [48] I.M.M.A. Shabaka, R.D. Metha, and P. Bradshaw. Longitudinal vortices imbedded in turbulent boundary layers. part 1. single vortex. *Journal of Fluid Mechanics*, 155:37–57, 1985.
- [49] H. Shim, Y.H. Jo, K. Chang, and K.J. Kwon. Wake characteristics of vane-type vortex generators in a flat plate laminar boundary layer. *Intl J. of Aeronautical Space Sci.*, 16:3, 2015.
- [50] F.T. Smith. Theoretical prediction and desing for vortex generators in turbulent boundary layers. *Journal of Fluid Mechanics*, 270:91–131, 1994.
- [51] N.N. Sorensen, F. Zahle, C. Bak, and T. Vronsky. Prediction of the effect of vortex generators on airfoil performance. *J. Phys. Conf. Ser.*, 524:012019, 2014.
- [52] H.H. Squire. The growth of a vortex in turbulent flow. *Aeronautical Quarterly*, 16:302–306, 1965.
- [53] F. Stilffried, S. Wallin, and A.V. Johansson. An improved passive vortex generator model for flow separation control. In *5th Flow Control Conference*, volume AIAA-2010-5091, 2010.
- [54] F. Stilffried, S. Wallin, and A.V. Johansson. Statistical vortex-generator-jet model for turbulent flow separation control. *AIAA Journal*, 51 (5):1119–1129, 2013.
- [55] W.A. Timmer. An overview of naca 6-digit airfoil series characteristics with reference to airfoils for large wind turbine blades. In *47th AIAA Aerospace Sciences Meeting*, volume AIAA 2009-268, 2009.
- [56] W.A. Timmer and R.P.J.O.M. van Rooij. Summary of delft university wind turbine dedicated airfoils. In *41st Aerospace Sciences Meeting and Exhibit*, volume AIAA 2003-352, 2003.
- [57] L. Ting, R. Klein, and O.M. Knio. *Vortex Dominated Flows*. Springer, 2007.
- [58] O. Tornblom and A.V. Johansson. A reynolds stress closure description of separation control with vortex generators in a plane asymmetric diffuser. *Physics of Fluids*, 19:115108, 2007.
- [59] N. Troldborg, N.N. Srensen, F. Zahle, and P.E. Rethore. Simulation of a mw rotor equipped with vortex generators using cfd and an actuator shape model. In *53rd AIAA Aerospace Sciences Meeting*, volume AIAA 2015-1035, 2015.

- [60] R.P.J.O.M. van Rooij. Modification of the boundary layer calculation in rfoil for improved airfoil stall prediction. Technical report, Delft University of Technology, Rapport IW-96087R, 1996.
- [61] C.M. Velte. Vortex generator flow model based on self-similarity. *AIAA Journal*, 51 (2):526–529, 2013.
- [62] C.M. Velte, M.O.L. Hansen, K.E. Meyer, and P. Fuglsang. Evaluation of the performance of vortex generators on the du 91-w2-250 profile using stereoscopic piv. In *WMSCI 2008: 12th World Multi-Conference on Systemics, Cybernetics and Informatics*, volume 2, 2008.
- [63] K.A. Waithe. Source term model for an array of vortex generator vanes. Technical report, NASA CR-2003-21215, 2003.
- [64] F Wallin and L.E. Eriksson. A tuning-free body-force vortex generator model. In *44th AIAA Aerospace Sciences Meeting*, volume AIAA-2006-873, 2006.
- [65] B.J. Wendt. Initial peak vorticity behavior for vortices shed from airfoil vortex generators. In *36th AIAA Aerospace Sciences Meeting and Exhibit*, 1997.
- [66] B.J. Wendt. Initial circulation and peak vorticity of vortices shed from airfoil vortex generators. Technical report, NASA CR-2001-211144, 2001.
- [67] B.J. Wendt, B.A. Reicher, and J.D. Foster. The decay of longitudinal vortices shed from airfoil vortex generators. Technical report, NASA CR-198356, 1995.
- [68] J.J. Wendt. Parametric study of vortices shed from airfoil vortex generators. *AIAA Journal*, 42 (11):2185–2195, 1965.
- [69] R.V Westphal, Pauley W.R., and J.K. Eaton. Interaction between a vortex and turbulent boundary. Technical report, NASA TM-88361, 1987.
- [70] F. Zahle, C. Bak, N. Sorensen, T. Vronsky, and N. Gaudern. Design of the lrp airfoil series using 2d cfd. *J. Phys. Conf. Ser.*, 524:012020, 2014.

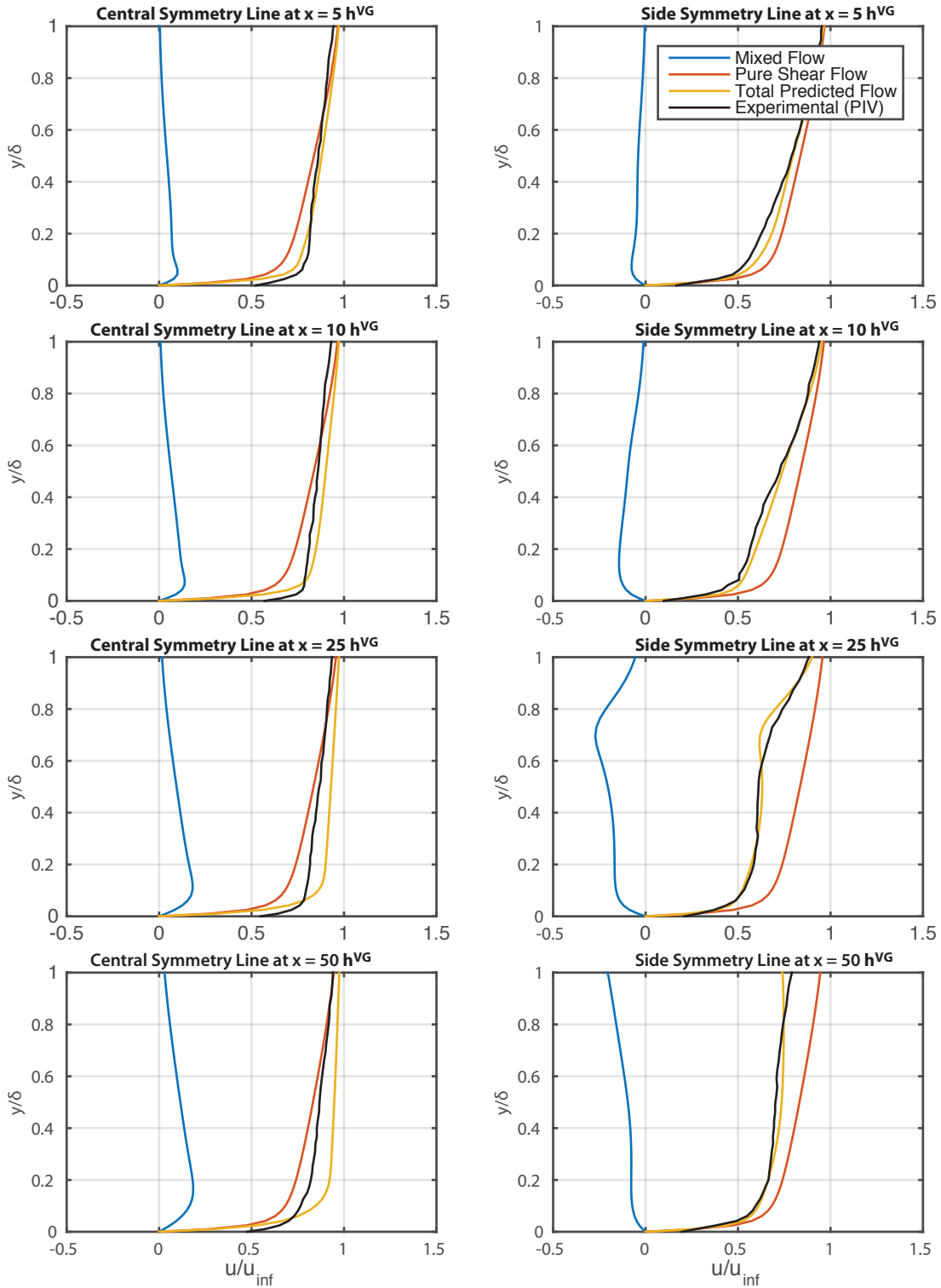


Figure 6: Measured and Reconstructed Velocity Profiles for Actuated Flow under the conditions described in table 1. The central symmetry line is located at $x/S = 0$ and the chosen side symmetry line is located along the $x/S = -1$ plane.

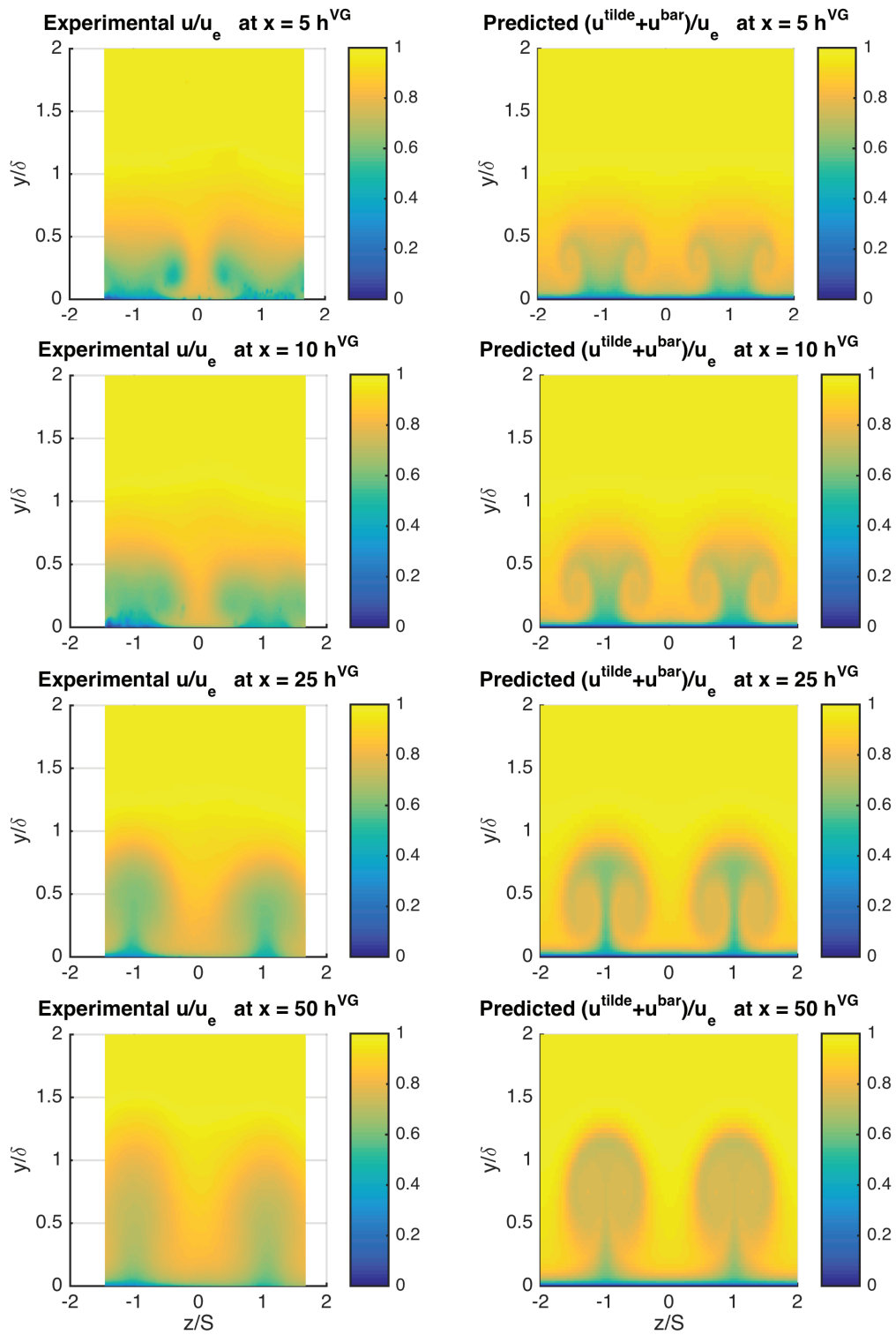


Figure 7: Measured and Reconstructed Velocity Profiles